

CHEMISTRY

Late-stage modification of complex drug: Base-controlled Pd-catalyzed regioselective synthesis and bioactivity of arylated osimertinibs

Rui Feng^{1†}, Yong-Qi Zhen^{2†}, Dongbo Wu^{3†}, Lian Sun¹, Jin-Bu Xu¹, Xiaohuan Li^{1*}, Lan Zhang^{1*}, Feng Gao^{1*}

Achieving regioselective synthesis in complex molecules with multiple reactive sites remains a tremendous challenge in synthetic chemistry. Regiodivergent palladium-catalyzed C–H arylation of complex antitumor drug osimertinib with various aryl bromides via the late-stage functionalization strategy was demonstrated here. This reaction displayed a switch in regioselectivity under complete base control. Potassium carbonate (K₂CO₃) promoted the arylation of acrylamide terminal C(sp²)-H, affording 34 derivatives. Conversely, sodium *tert*-butoxide (t-BuONa) mediated the aryl C(sp²)-H arylation of the indole C2 position, providing 27 derivatives. The derivative **3r** containing a 3-fluorophenyl group at the indole C2 position demonstrated similar inhibition of EGFR^{T790M/L858R} and superior antiproliferative activity in H1975 cells compared to osimertinib, as well as similar antiproliferative activity in A549 cells and antitumor efficacy in xenograft mouse model bearing H1975 cells. This approach provides a “one substrate–multi reactions–multiple products” strategy for the structural modification of complex drug molecules, creating more opportunities for the fast screening of pharmaceutical molecules.

INTRODUCTION

Drug development is a complex, costly, and time-consuming process that can take 10 to 15 years or even longer (1–4). As a key enabler, chemical synthesis is an essential step in the drug discovery process. Innovations in synthetic methodologies can greatly facilitate the construction of diverse and drug-like compound libraries (5). Over the past decade, late-stage functionalization (LSF), which could directly modify high-complexity, drug-like substrates at a late stage, has been an efficient way to prepare new chemical entities for drug discovery and chemical biology, without resorting to *de novo* synthesis (5–7). Transition metal-catalyzed C–H bond activation approaches allow the installation of handles for further derivatization and offer the opportunity to explore chemical space more effectively than relying solely on conventional synthetic approaches, creating the possibility of broad adoption of LSF (8). However, the multitude of C–H bonds in structurally complex biologically active molecules could drastically limit the applicability of C–H bond activations since the regioselectivity of the LSF is crucial. The regioselectivity of a particular compound could greatly affect the biological activity of its derivatives.

As an oral, unique mono-anilino-pyrimidine epidermal growth factor receptor kinase inhibitor (EGFR TKI), osimertinib (Fig. 1A) was approved by the US Food and Drug Administration in November 2015 as a first-line treatment for non-small cell lung cancer (NSCLC) patients with EGFR activation and/or resistant mutations (9). Osimertinib is effective in overcoming or delaying drug resistance associated with first-generation EGFR TKIs and reducing nonselectivity toxicity mediated by EGFR TKIs (10, 11). However,

after approximately 19 months of treatment with osimertinib, acquired resistance also occurs, often associated with the C797S point mutation and/or other mechanisms (12). In addition, increasing the dosage of osimertinib to overcome the C797S mutation by enhancing competition with adenosine triphosphate (ATP) is not a feasible solution, as the main metabolite of osimertinib has been shown in human pharmacokinetic studies to result in poor *in vivo* selectivity and increased risk of toxicity associated with wild-type EGFR TKIs (13, 14). To address these limitations, many osimertinib derivatives have been developed, but there is still a need for further discovery in this area (15–21).

Osimertinib can be divided into four important parts as an EGFR TKI (Fig. 1B). The indole ring, which is embedded deeply in the hydrophobic pocket of the EGFR protein, selectively inhibits EGFR^{T790M} kinase by interacting with the Met⁷⁹⁰ residue of the kinase through van der Waals forces. The Michael acceptor acrylamide side chain extends toward the conserved residue Cys⁷⁹⁷ in the active site and forms a covalent bond with the amino acid residue Cys⁷⁹⁷ through Michael addition. The pyrimidine ring is located in the hinge region and is close to the Met⁷⁹³ residue while being distant from the Gatekeeper residue Met⁷⁹⁰. Optimizing those parts can lead to the development of more effective and selective EGFR TKIs. The nitrogen atom at position 1 and the bridging hydrogen atom of the pyrimidine ring of osimertinib engage in a bidentate hydrogen bond with the hydrogen and oxygen atoms, respectively, on the Met⁷⁹³ residue located in the hinge region of the EGFR protein (22, 23). Inspired by the information above, we sought to introduce additional hydrophobic groups at the indole C2 position of osimertinib to occupy the hydrophobic pocket at the rear of the ATP binding site, which could strengthen the interaction between osimertinib and the ATP binding site or Met⁷⁹⁰ residues, for enhancing selectivity. Considering the crucial role of the aryl ring in the field of antitumor drug development, as well as its contribution to the hydrophobicity (24, 25), we hypothesized that introducing the aryl ring with various substituted groups to the indole C2 position may enhance the interactions of osimertinib with corresponding amino acid residues.

¹Sichuan Engineering Research Center for Biomimetic Synthesis of Natural Drugs, School of Life Science and Engineering, Southwest Jiaotong University, Chengdu 610031, P.R. China. ²State Key Laboratory of Biotherapy and Cancer Center, West China Hospital, Sichuan University, Chengdu 610041, P.R. China. ³Center of Infectious Diseases, West China Hospital, Sichuan University, Chengdu 610041, P.R. China.

*Corresponding author. Email: xiaohuanli@swjtu.edu.cn (X.L.); zhanglanx_9@126.com (L.Z.); gaof@swjtu.edu.cn (F.G.)

†These authors contributed equally to this work.

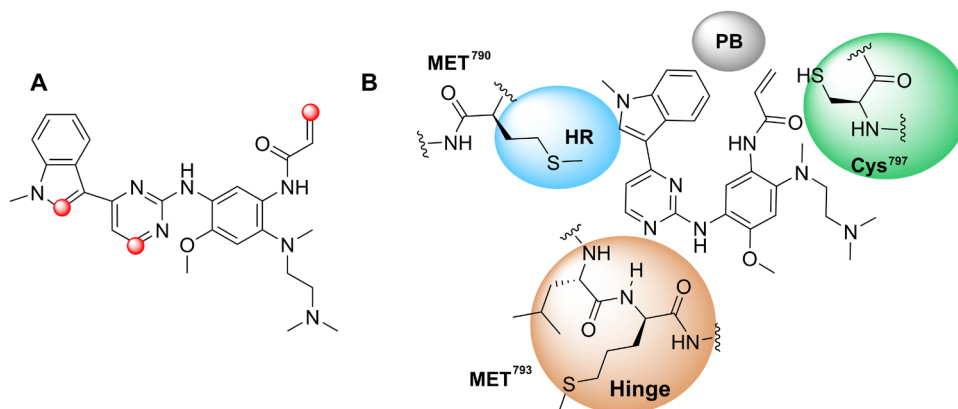


Fig. 1. Overview of osimertinib. (A) Structure of osimertinib and its active sites. (B) Two-dimensional binding mode of osimertinib to EGFR found in the x-ray structure. HR, hydrophobic region; PB, phosphate binding site.

A great deal of effort has been devoted to the formation of C2-arylated indole via transition metal-catalyzed oxidative C—H bond activation (26–28). The method avoids the prefunctionalization of indoles and affords a shortcut for the arylation of indoles (29). The coupling species including aryl halides, hypervalent iodine arylating agents, arylsiloxanes, aryl boronic acids, aryltrifluoroborate salts, aromatic sulfinic acids, aryltriazenes, and even arenes have been successfully used as the aryl sources, while the transition metal like palladium, rhodium, copper, ruthenium, nickel, and cobalt have been applied in the direct arylation of indoles (29–40). Nevertheless, direct arylation for the synthesis of 2-aryl indoles still faces the regioselectivity challenge as the most reactive position of indoles is the C3 site (41). Strategies in achieving high site selectivity of indole C2 arylation include preinstallation of directing groups or protecting groups on the nitrogen atom, the use of acidic/basic additives, the switch of ligand, and the limited substrate scope (42).

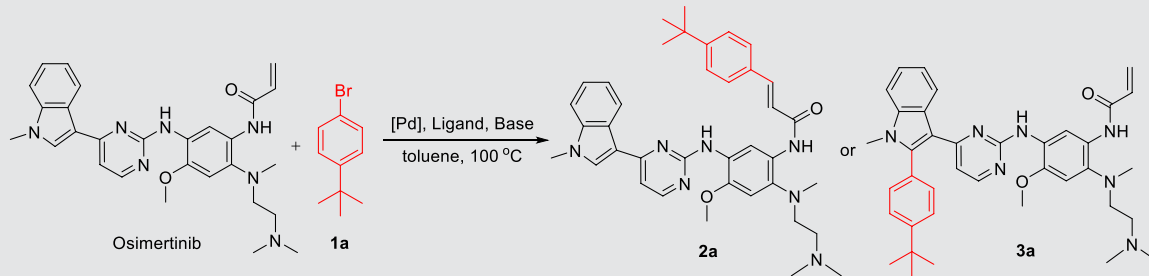
The LSF strategy appears to be an efficient method to introduce the aryl ring into the indole motif of osimertinib. However, since osimertinib is a complex drug molecule with three aromatic rings and multiple functional groups, introducing the aromatic ring to the indole C2 position via C—H activation requires selectivity since it can occur at the double bond located in the acrylamide side chain as well as the pyrimidine ring (43, 44). In particular, a Heck reaction on the acrylamide should be easier to access. Both C—H activation of indole C2 position and Heck reaction can use the palladium catalytic system with base, and even the same catalytic system was adopted in the two reactions. For example, Young and coworkers used PdCl₂(PPh₃)₂/potassium acetate to complete the indole C2 arylation in the search of new antimicrobial agents, while the same catalytic system was applied to a Heck reaction to couple 1-(pyrrolidin-1-yl) prop-2-en-1-one and 5-bromo isatin by Yu and coauthors (45, 46). More examples are that the same palladium catalysts and different bases could achieve indole C2 C—H activation or Heck reaction of acrylamide, respectively (43, 47–51). As said above, we aimed to synthesize a series of indole C2-arylated osimertinib derivatives by LSF strategy. The key issue of the strategy was how to control the regioselectivity. Here, we report the base-controlled switching of regioselectivity between the C2 position of the indole ring and the terminal double bond of the acrylamide side chain in the structurally complex antitumor drug osimertinib and evaluate the antitumor activity of the synthesized derivatives.

RESULTS

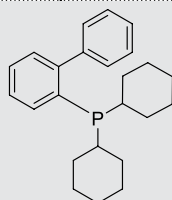
Reaction condition optimization

The initial investigation commenced with osimertinib and 1-bromo-4-(*tert*-butyl)benzene **1a** as model substrates and toluene as solvent, keeping the reaction temperature at 100°C (Table 1). At first, we used Pd(OAc)₂ as the catalyst and Cy-John-Phos or PCy₃ as the ligand to screen the base (entries 1 to 7) (52). Only one product was observed in the cases of using inorganic bases K₂CO₃, CsF, and Cs₂CO₃ (entries 1 and 5, 2, and 6), whereas the organic bases *t*-BuOK and sodium bis(trimethylsilyl)amide (NaHMDS) failed to produce any products. The molecular formula of the formed product was deduced as C₂₈H₃₃N₇O₂ based on a protonated molecular ion at *m/z* 632.3635 [M + H]⁺ in the high resolution electrospray ionization mass spectroscopy (HRESIMS) (calcd 632.3645). Compared to the starting material osimertinib, the proton signals of the *tert*-butylphenyl group were observed and the terminal double bond disappeared in the ¹H nuclear magnetic resonance (NMR) spectrum, indicating that **1a** was coupled with the acrylamide terminal double bond of osimertinib to generate the product **2a** only. The coupling constant of the double bond in the acrylamide side chain was 15.6 Hz, revealing that the substituted double bond was (*E*) stereoselectivity. The results proved the positive effect of the inorganic base on coupling the acrylamide terminal double bond with **1a**. However, using K₂CO₃ as base and replacement of Pd(OAc)₂ with Pd₂(dba)₃, and Cy-John-Phos or PCy₃ with 2,2'-bis(diphenylphosphino)-1,1'-binaphthalene (BINAP), no product was detected (entry 8). Pleasingly, in the presence of *t*-BuOK or *t*-BuONa with Pd₂(dba)₃/BINAP, the reactions gave the indole C2 coupling product **3a** as the only detectable product (entries 9 and 10), suggesting that the organic base might be beneficial to the C—H activation of indole C2 position. Besides ¹H and ¹³C NMR spectra, the structure of target compound **3a** was confirmed by x-ray diffraction (Fig. 2A). Similarly, the reaction did not yield any products when NaHMDS was used (entry 11). To our delight, when applying Pd(PPh₃)₄ directly as catalyst, *t*-BuOK as base only obtained **3a** in 49% yield, while K₂CO₃ only gave **2a** in 65% yield (entries 12 and 13). The results preliminarily demonstrated that the regioselective of C—H activation at both reaction sites of osimertinib could be achieved by base control, which might be due to the different roles the base plays in the Heck reaction and the indole C2 C—H activation (53). Heck reaction might be through a carbometallation pathway that requires

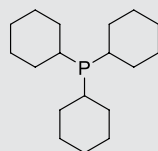
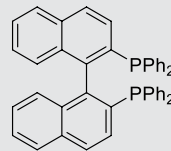
Table 1. Optimization of the reaction conditions. Reaction conditions: If not specified, osimertinib (0.1 mmol), **1a** (0.2 mmol), catalyst Pd(OAc)₂ (5 mol %), Pd₂(dba)₃ (5 mol %), Pd(PPh₃)₄ (10 mol %), ligand (10 mol %), base (0.2 mmol), toluene (1 ml), 20 hours.



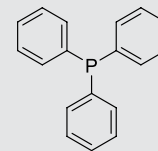
Entry	Catalyst	Ligand	Base	Yield of 2a (%)*	Yield of 3a (%)*
1	Pd(OAc) ₂	Cy-John-Phos	K ₂ CO ₃	62	–
2	Pd(OAc) ₂	Cy-John-Phos	CsF	58	–
3	Pd(OAc) ₂	Cy-John-Phos	<i>t</i> -BuOK	–	–
4	Pd(OAc) ₂	Cy-John-Phos	NaHMDS	–	–
5	Pd(OAc) ₂	PCy ₃	K ₂ CO ₃	45	–
6	Pd(OAc) ₂	PCy ₃	Cs ₂ CO ₃	49	–
7	Pd(OAc) ₂	PCy ₃	<i>t</i> -BuONa	–	–
8	Pd ₂ (dba) ₃	BINAP	K ₂ CO ₃	–	–
9	Pd ₂ (dba) ₃	BINAP	<i>t</i> -BuOK	–	56
10	Pd ₂ (dba) ₃	BINAP	<i>t</i> -BuONa	–	55
11	Pd ₂ (dba) ₃	BINAP	NaHMDS	–	–
12	Pd(PPh ₃) ₄	–	<i>t</i> -BuOK	–	49
13	Pd(PPh ₃) ₄	–	K ₂ CO ₃	65	–
14	Pd(PPh ₃) ₄	–	<i>t</i> -BuONa	–	54
15	Pd(PPh ₃) ₄	–	<i>t</i> -BuOLi	–	–
16	Pd(PPh ₃) ₄	–	CsF	56	–
17	Pd(PPh ₃) ₄	–	Cs ₂ CO ₃	58	–
18	Pd(PPh ₃) ₄	–	LiHMDS	–	–
19	Pd(PPh ₃) ₄	–	NaHMDS	–	–
20	Pd(PPh ₃) ₄ [†]	–	<i>t</i> -BuONa	–	58
21	Pd(PPh ₃) ₄ [†]	–	<i>t</i> -BuONa [‡]	–	60
22	Pd(PPh ₃) ₄ [†]	–	K ₂ CO ₃	64	–
23	Pd(PPh ₃) ₄ [†]	–	K ₂ CO ₃ [‡]	63	–



Cy-John-Phos

PCy₃

BINAP

PPh₃

*Isolated yield. †A value of 20 mol %. ‡A value of 0.3 mmol.

anti-dehydropalladation associated with base. The C2 arylation of indole might be by the electrophilic pathway that involves the electrophilic addition of an aryl-palladium species to the indole C3 position, a 1,2-migration (C3 to C2 migration) of the palladium center, a deprotonation associated by base, and the reductive elimination of palladium metalation intermediate (54). The stronger organic base *t*-BuOK might promote the deprotonation of the indole

motif. However, the base-controlled selectivity may refer to the distinguished structure of osimertinib. The pyrimidine ring at the indole C3 position may have some effect on the selectivity since when simple indole or acrylamide was used as substrates, the corresponding palladium catalytic system did not work.

We next investigated the influence of different bases on the reaction process with the catalyst Pd(PPh₃)₄. The reaction using *t*-BuONa

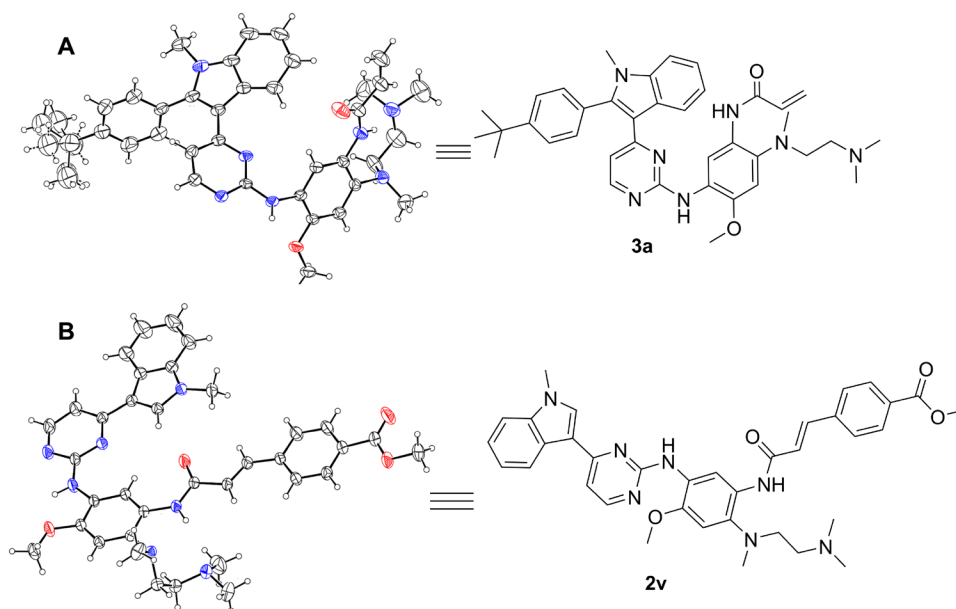


Fig. 2. Single-crystal x-ray structures of compounds **3a** and **2v**. (A) **3a** and (B) **2v**.

only produced **3a** in 54% yield, which was better than *t*-BuOK (entries 14 and 12). CsF and Cs₂CO₃ only gave **2a** but led to little drops in the yields (entries 16 and 17). Other bases including *t*-BuOLi, lithium bis(trimethylsilyl)amide (LiHMDS), and NaHMDS did not provide any products, and the starting material remained. In addition, the yield of compound **3a** rose a little to 60% when increasing the amount of Pd(PPh₃)₄ to 20 mol % along with the amount of *t*-BuONa to three equivalents. However, the yield of **2a** was nearly not influenced by the amounts of Pd(PPh₃)₄ and K₂CO₃ (entries 20 to 23). Thus, the optimized conditions for the generation of desired compounds **2a** and **3a** are those in entries 13 and 21 (Table 1), respectively.

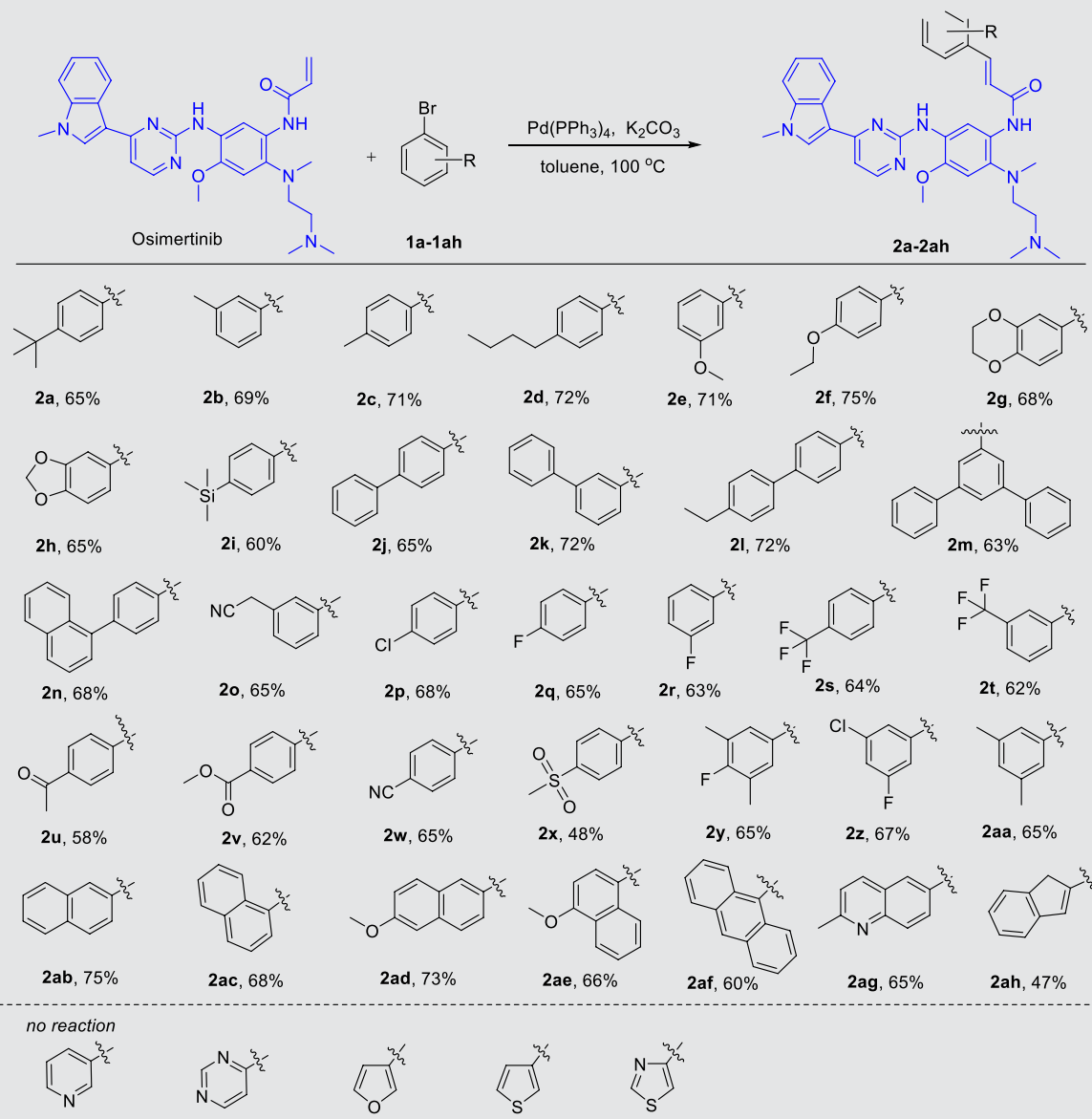
Substrate scope

With the optimized conditions for the base-controlled regioselective Heck coupling and the indole C2 C–H activation in hand, we evaluated the scope of the reactions by assessing combinations of various aryl bromides with osimertinib. First, under optimal conditions for the coupling of the terminal double bond with aryl bromides using K₂CO₃, a broad range of electron-withdrawing and electron-donating substituents in the benzene ring, at positions *para*- and *meta*-, with respect to the bromine atom, were tolerated (Table 2). The substrates **1a** to **1d** with alkyl groups on the phenyl ring delivered the corresponding products in good results (65 to 72% yields), as well as substrates with alkoxy, trimethyl silyl, (substituted)phenyl, or naphthyl group on the phenyl ring (**1e** to **1o**, 60 to 75% yields). The coupling process for **1p** to **1w**, where the stronger electron-withdrawing groups such as chloro, fluoro, trifluoromethyl, and cyanide were present at *para*- or *meta*-position in aryl moiety, proceeded smoothly (58 to 68% yields). When the methylsulfonyl group was substituted at *para*-position (**1x**), the yield of the coupling products was moderate (48%). The trisubstituted or disubstituted benzenes including 5-bromo-2-fluoro-1,3-dimethyl-benzene (**1y**), 1-bromo-3-chloro-5-fluorobenzene (**1z**), and 1-bromo-3,5-dimethylbenzene (**1aa**) were well tolerated, leading to coupling products **2y**, **2z**, and **2aa** in yield 65, 67, and 65%, respectively. The aforementioned results suggest that

the electronegativity and the substituted positions of the bromobenzene do not affect the coupling reaction. The optimal conditions were also applicable for bromonaphthalene and its derivatives, bromoanthracene, 6-bromo-2-methylquinoline, and 2-methyl-1*H*-indene, delivering the corresponding products (**2ab** to **2ah**) in 47 to 75% yields. However, heteroaryl bromides such as pyridine, pyrimidine, furan, thiophene, and thiazole did not react with osimertinib under optimal conditions. In addition, to further confirm the structures of this series of compounds, x-ray diffraction analysis was performed on compound **2v** (Fig. 2B), confirming that the products under the catalysis of Pd(PPh₃)₄/K₂CO₃ are arylated derivatives of osimertinib at the terminal double bond in the side chain.

The scope of osimertinib indole C2 selective arylation with Pd(PPh₃)₄/*t*-BuONa was examined as well (Table 3). Similarly, the aryl bromides that bear both electron-donating groups, such as alkyl (**1a**, **1b**, **1d**, and **1ai**), alkoxy (**1e** to **1h** and **1ak**), phenyl (**1j** to **1l**), pyridinyl (**1al**), and naphthyl (**1n**), as well as electron-withdrawing groups, such as chloro (**1p**), fluoro (**1q** and **1r**), and trifluoromethyl (**1s** and **1t**), were tolerated in the standard reaction conditions, affording the desired indole C2 coupling products in good yields (53 to 65%). Trisubstituted and disubstituted phenyl bromides with electron-withdrawing or electron-donating groups (**1y**, **1aa**, and **1aj**) furnished desired products with 52 to 57% yields. Furthermore, naphthyl bromides and those bearing the methoxy group provided the cross-coupling products (**3ab** to **3ae**) in 57 to 61% yields. 6-Bromoquinoline (**1am**) is also reactive under identical reaction conditions to obtain the cross-coupling product in 56% yield. The reactivity of the various tested aryl bromides was no different, indicating the good applicability of the optimal reaction conditions. However, bulky substrates such as 9-bromo anthracene, 2-bromo-1,3-dimethyl-benzene, and 2,4,6-trisopropyl benzene did not produce any products under the conditions, suggesting that aryl bromides with large steric hindrance were not applicable in indole C2 cross-coupling process. In addition, heteroaryl bromides including pyridine, pyrimidine, furan, and thiophene exhibited low reactivity under this catalytic system.

Table 2. Substrate scope of aryl bromides for the base-controlled regioselective Heck coupling of the terminal double bond in the acrylamide sidechain of osimertinib. Reaction conditions: osimertinib (0.1 mmol), **1a** to **1ah** (0.2 mmol), Pd(PPh₃)₄ (10 mol %), K₂CO₃ (0.2 mmol), toluene (1 ml), 20 hours. Isolated yield.

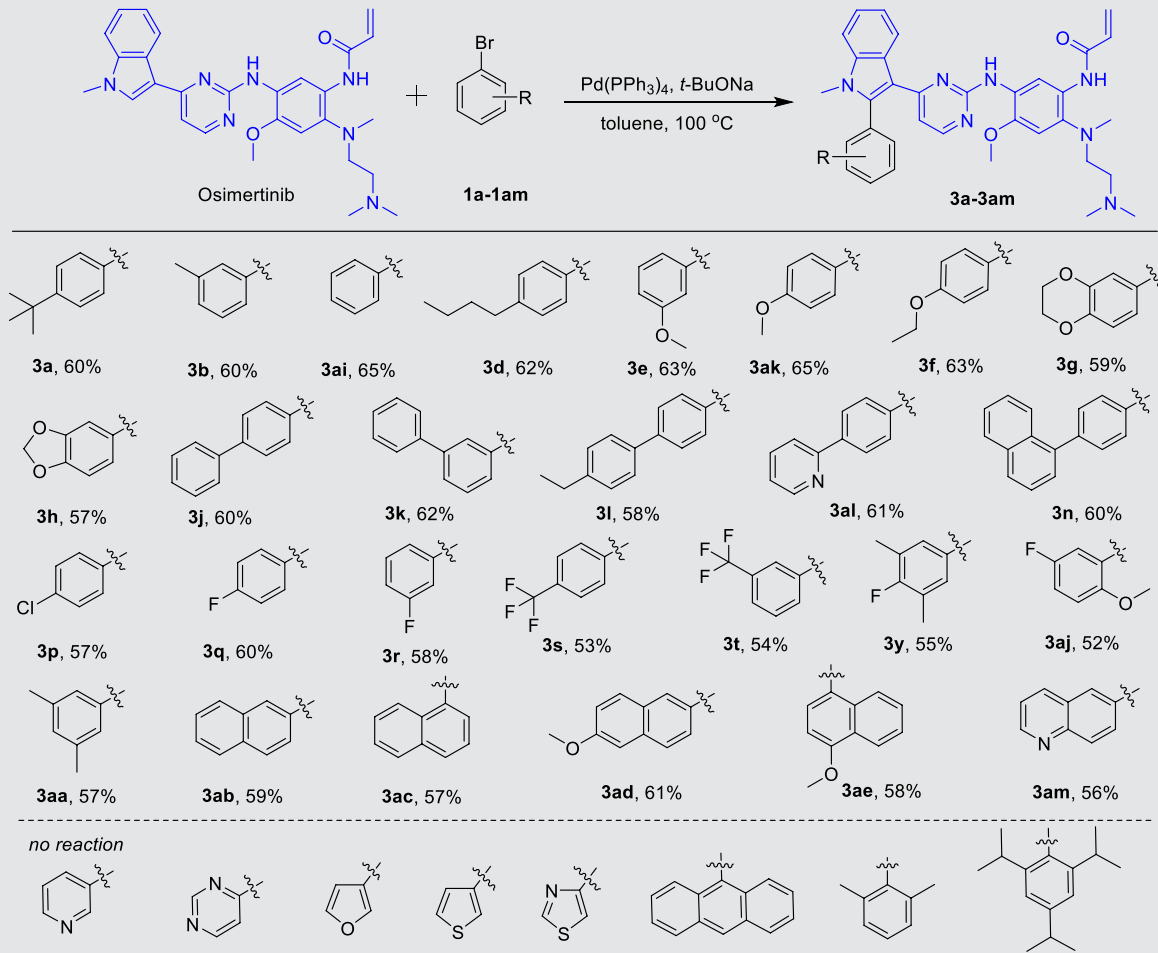


The synthetic utility of the present base-controlled regioselective synthesis of osimertinib was further demonstrated by two large-scale reactions. Accordingly, the reaction was carried out using osimertinib (1.0 mmol), 4-*tert*-butyl bromobenzene (2.0 mmol), Pd(PPh₃)₄ (10 mol %), and K₂CO₃ (2.0 mmol), which delivered the desired product **2a** in 63% yield. When conducting the reaction of osimertinib (1.0 mmol) with 4-*tert*-butyl bromobenzene (2.0 mmol), Pd(PPh₃)₄ (20 mol %), and *t*-BuONa (3.0 mmol), 368 mg of **2a** was obtained (58% yield). The two large-scale reactions were essentially the same yield as the small-scale reactions in Tables 2 and 3.

In vitro antiproliferative activity on H1975 and A549 cells

Using osimertinib as a positive control, the in vitro antiproliferative activity of 61 newly synthesized derivatives of osimertinib against H1975 (EGFR^{T790M/L858R}) cells were used by the 3-(4,5-dimethylthiazol-2-yl)-2,5-diphenyltetrazolium bromide (MTT) assay (table S1). The results showed that 21 compounds (**2f** to **2i**, **2p**, **2r** to **2u**, **2z**, **2ab**, **2ag**, **2ah**, **3e**, **3g**, **3h**, **3k**, **3p**, **3r**, **3s**, and **3ab**) had similar or better percent inhibition than osimertinib at the concentration of 0.5 μM against H1975 cells. Substituents on the aromatic ring have an impact on the cytotoxicity. Introducing the mono- or disubstituted phenyl ring with electron-donating groups (alkyl, alkoxy,

Table 3. Substrate scope of aryl bromides for the base-controlled regioselective C–H activation of C2 position at the indole moiety of osimertinib.
Reaction conditions: osimertinib (0.1 mmol), **1a** to **1am** (0.2 mmol), Pd(PPh₃)₄ (20 mol %), *t*-BuONa (0.3 mmol), toluene (1 ml), 20 hours. Isolated yield.



phenyl, and trimethylsilyl groups) to both acrylamide and indole C2 position reduced the percent inhibition of osimertinib, except for compound **3e** with *meta*-methoxy benzene ring at the indole C2 position. Both 2,3-dihydrobenzo[*b*][1,4]dioxine and benzo[*d*][1,3]dioxole substituted at acrylamide position enhanced the percent inhibition notably (**2g** and **2h**), whereas 2,3-dihydrobenzo[*b*][1,4]dioxine (**3g**) at the indole C2 position led to slight decrease, but enzo[*d*][1,3]dioxole increased the percent inhibition (**3h**). For acrylamide derivatives, compound **2p** with *para*-chlorobenzene ring, **2s** and **2t** with *para*- or *meta*-trifluoromethyl benzene ring, and **2z** with both chlorine and fluorine atoms showed better activities than compounds with fluorine atom (**2q** and **2r**) and other electron-withdrawing groups (**2u** to **2x**). When naphthyl group was introduced to osimertinib, the effect of activity was influenced by the substituted position. 2-Naphthyl group enhanced the percent inhibition (**2ab**), and 1-naphthyl group decreased the activity (**2ac**). Moreover, for the substituted naphthyl group, the connected positions to osimertinib were not important. Both compounds **2ad** and **2ae** exhibited less activity than osimertinib. The indole C2 derivatives (**3p** to **3t**, and **3ab** to **3ae**) had the same structure-activity relationship, except for **3r** and **3t**. On the contrary,

compound **3r** containing *meta*-fluoro benzene ring enhanced the cytotoxicity, while **3t** with *meta*-trifluoromethyl benzene ring decreased the percent inhibition rate. Meanwhile, when choosing quinolyl group as a substituent, the acrylamide derivative **2ag** displayed better cytotoxicity than osimertinib, whereas indole C2 derivative **3am** promoted the growth of H1975 cells. Following the assessment of inhibitory rates at 0.5 μM against H1975 cells, 14 compounds with promising activity were selected for further median inhibitory concentration (IC₅₀) determination in both A549 and H1975 cell lines (Table 4).

According to Table 4, most selected modified compounds exhibited better or equal antiproliferative activities against both A549 and H1975 cell lines. For A549 cells, all selected compounds had better IC₅₀ values than osimertinib. Except for **2z** (IC₅₀ = 0.4333 μM), the IC₅₀ values of all acrylamide derivatives are less than half of osimertinib (IC₅₀ = 0.6864 μM), whereas the acrylamide derivatives **2ab** and **2ag** featuring naphthyl and quinolyl groups showed the best activity. On the contrary, when the naphthyl or quinolyl group attached to the indole C2 position, the activity was decreased. For H1975 cells, the introduction of particular aromatic ring to indole C2 position enhanced the activity, whereas the modification of acrylamide showed a

Table 4. Antiproliferative activities against A549 and H1975 cell lines in vitro.

Compound	IC ₅₀ (μM)	
	A549 (EGFR ^{WT})	H1975 (EGFR ^{L858R/T790M})
2g	0.2072 ± 0.0020	0.1210 ± 0.0019
2h	0.2954 ± 0.0018	0.1050 ± 0.0009
2p	0.2954 ± 0.0032	0.2506 ± 0.0026
2s	0.2072 ± 0.0018	0.7164 ± 0.0045
2z	0.4333 ± 0.0071	0.2548 ± 0.0027
2ab	0.1151 ± 0.0013	0.5768 ± 0.0031
2ag	0.1139 ± 0.0023	0.3996 ± 0.0016
3e	0.3009 ± 0.0022	0.0783 ± 0.0006
3h	1.1076 ± 0.0112	0.3740 ± 0.0022
3k	0.4001 ± 0.0049	0.1386 ± 0.0027
3p	0.4151 ± 0.0010	0.1065 ± 0.0023
3r	0.4333 ± 0.0019	0.0438 ± 0.0005
3s	0.4139 ± 0.0011	0.0969 ± 0.0008
3ab	0.6520 ± 0.0054	0.2658 ± 0.0033
Osimertinib	0.6864 ± 0.0045	0.2100 ± 0.0034

similar IC₅₀ value to osimertinib. Derivatives **3p**, **3r**, and **3s** with halogen atoms on the benzene ring exhibited the best antiproliferative activities. In particular, the IC₅₀ value of **3r** was 0.044 μM, while the positive control osimertinib was 0.210 μM. In general, **2g**, **2h**, **3e**, **3p**, **3r**, and **3s** exhibited promising in vitro antiproliferative activity against both A549 and H1975 cell lines. On the basis of the distinct structural characteristics of these six compounds, we selected **2h**, **3e**, and **3r** for EGFR^{T790M/L858R} kinase activity testing.

In vitro EGFR kinase assays

The selected compounds were evaluated for their in vitro kinase inhibitory activity (Table 5). **2h** exhibited an IC₅₀ value obviously higher than the positive control drug osimertinib, possibly due to its modification on the double bond, which hinders its binding to the Cys⁷⁹⁷ protein and causes off-target effects. In contrast, **3e** and **3r** both showed IC₅₀ values comparable to osimertinib. Therefore, **3e** and **3r** were selected for further identification in the H1975 cells.

In vitro antiproliferative activity of **3r** and **3e** on osimertinib-resistant H1975 cells

To assess the effect of **3r** and **3e** on the growth of resistant cells, the antiproliferative activities of **3r**, **3e**, and osimertinib against osimertinib-resistant H1975 cells (H1975OR) were evaluated. As shown in fig. S1, the results suggested that **3r** exhibited a bit better antiproliferative activity (IC₅₀ = 1.9 μM) than osimertinib and **3e** (IC₅₀ = 2.6 μM for osimertinib, IC₅₀ = 3.9 μM for **3e**).

Effect on cell apoptosis

To assess the antiproliferative activity of compounds **3e** and **3r** in human NSCLC cells, cell colony formation assay was carried out. Presenting notable cell colony reduction and superior antiproliferative activity of **3r** than that of both **3e** and osimertinib at the same concentrations (Fig. 3A). For figuring out the mechanism of cell death induced by **3e** and **3r**, Hoechst 33258 staining was conducted,

Table 5. Inhibitory activities against EGFR kinases in vitro.

Compound	IC ₅₀ (nM)
	EGFR ^{L858R/T790M}
2h	1391 ± 360
3e	6 ± 3
3r	5 ± 2
Osimertinib	6 ± 2

resulting in a marked increase in fluorescence intensity, which was referred to as the destruction of cell structure and chromatin contraction (Fig. 3B). Subsequently, the apoptosis rate was detected by Annexin V/Propidium iodide (PI) double staining (Fig. 3C). The results showed that **3e** and **3r** could induce apoptosis. In addition, Western blot analysis revealed that the expression levels of Bax and cleaved caspase-3 were markedly up-regulated, while the antiapoptotic marker Bcl-2 was down-regulated after **3e** and **3r** treatment (Fig. 3D), confirming that **3e** and **3r** could notably induce apoptosis. Together, compounds **3e** and **3r** can inhibit the proliferation and induce apoptosis of H1975 cells, in which **3r** was superior to **3e** and osimertinib.

Effect on cell migration

Whether **3e** and **3r** can inhibit cell migration was determined by using wound healing scratch assay. The result showed that the wound closure rate of cells treated with **3e** and **3r** was reduced (Fig. 4A). Moreover, on the basis of Western blot analysis and immunofluorescence analysis, up-regulation of E-cadherin and down-regulation of matrix metalloproteinase-2 (MMP-2) in H1975 cells (Fig. 4, B to D) were observed. Overall, the above experimental

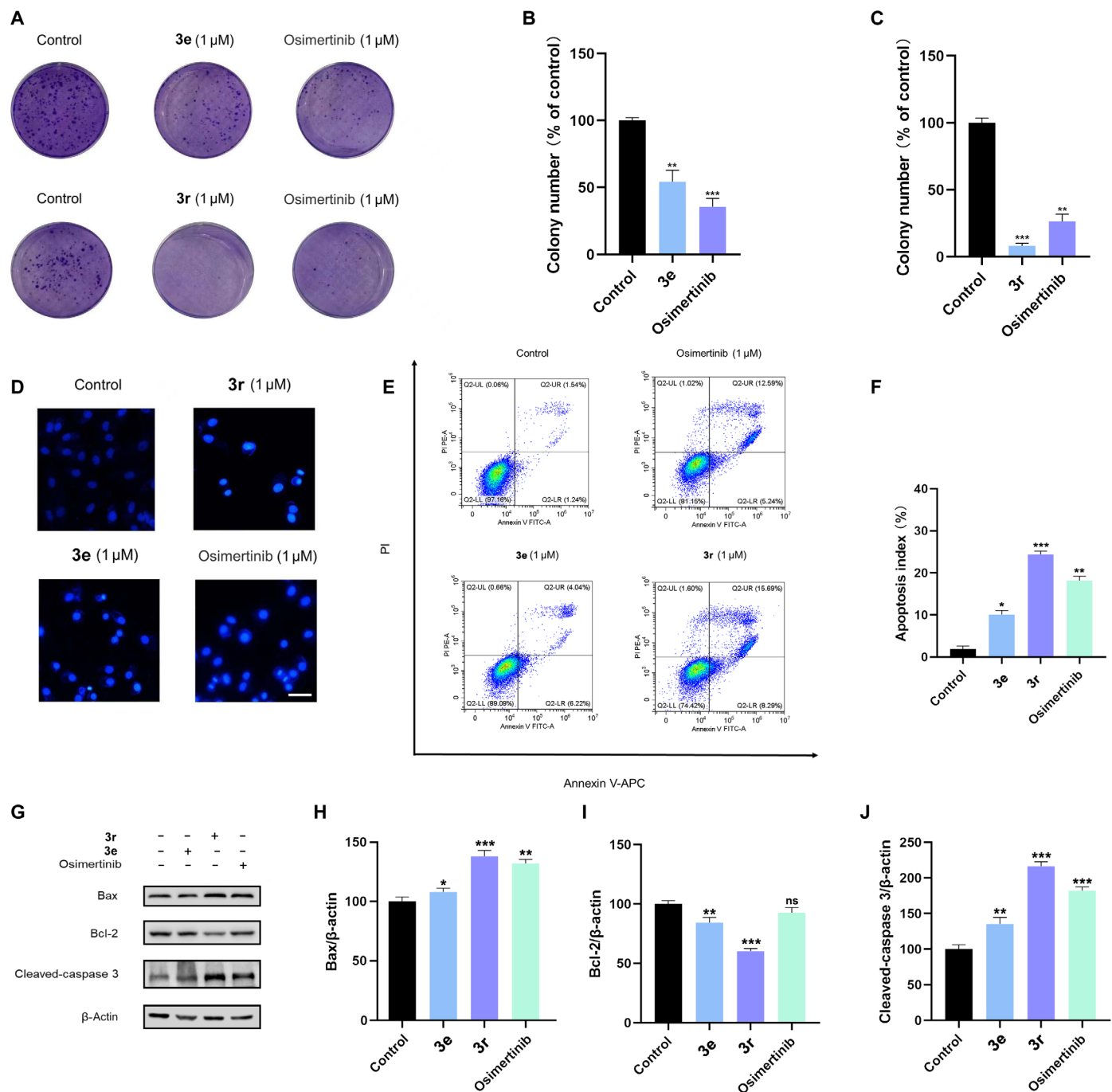


Fig. 3. Compounds 3e and 3r inhibited cell proliferation and induced apoptosis of H1975 cells. (A to C) Colony formation assay of H1975 cells treated with 3e, 3r, and osimertinib. (D) Hoechst 33258 staining assay in H1975 cells treated with 3e, 3r, and osimertinib. Scale bar, 40 μm. (E and F) H1975 cells were treated with 3e, 3r, and osimertinib for 24 hours, and apoptosis ratios were determined by flow cytometry analysis of Annexin V/PI double staining. (G to J) Western blot analysis of Bax, Bcl-2, and cleaved caspase-3 in H1975 cells treated with 3e, 3r, and osimertinib for 24 hours. β-Actin was used as a loading control. ns, not significant.

results indicated that 3e and 3r inhibited the migration of H1975 cells similarly to osimertinib.

In vivo antitumor efficacy study

The antitumor activity of osimertinib or 3r was investigated in H1975 xenograft mouse model. The measured tumor volume and

weight referred to the robust antitumor activity of 3r in H1975 xenograft mouse model, especially that the high dose (20 mg/kg) group was consistent with the antitumor effect of osimertinib (20 mg/kg) (Fig. 5, A to C). In addition, the Western blot analysis of Ki67 in tumor tissues also indicated that 3r could notably inhibit the proliferation of the H1975 xenograft mouse model (Fig. 5, D and E).

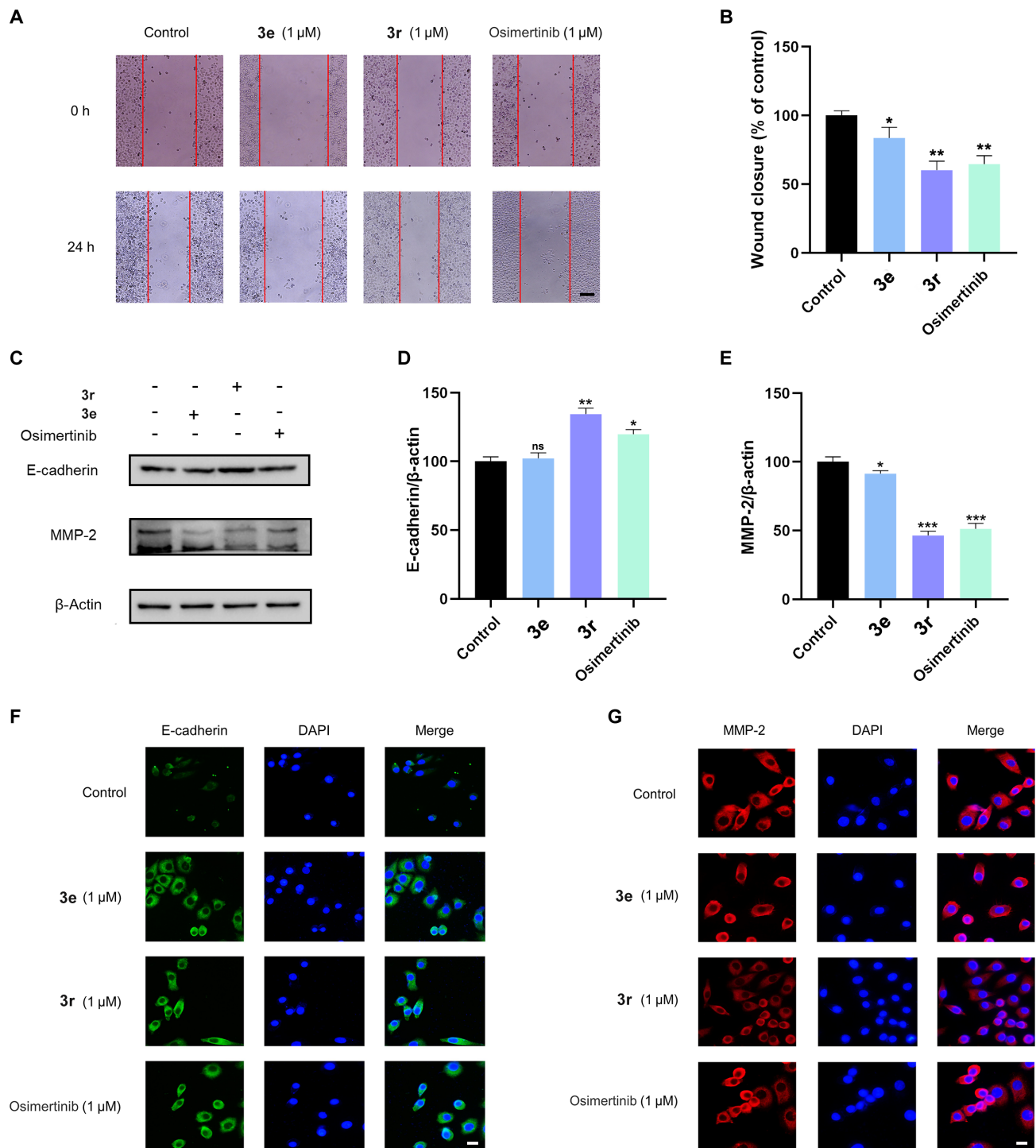


Fig. 4. Compounds 3e and 3r inhibit migration in H1975 cells. (A and B) H1975 cells were treated with 3e, 3r, and osimertinib. The scratch assay was used to measure migration capabilities of the cells. The wound closure ratio represents the level of cell migration ability. Scale bar, 100 μm. (C to E) Western blot analysis of E-cadherin and MMP-2 in H1975 cells treated with 3e, 3r, and osimertinib for 24 hours. β-Actin was used as a loading control. (F and G) Immunofluorescence analysis of MMP-2 and E-cadherin levels in H1975 cells treated with 3e, 3r, and osimertinib for 24 hours. Scale bar, 10 μm.

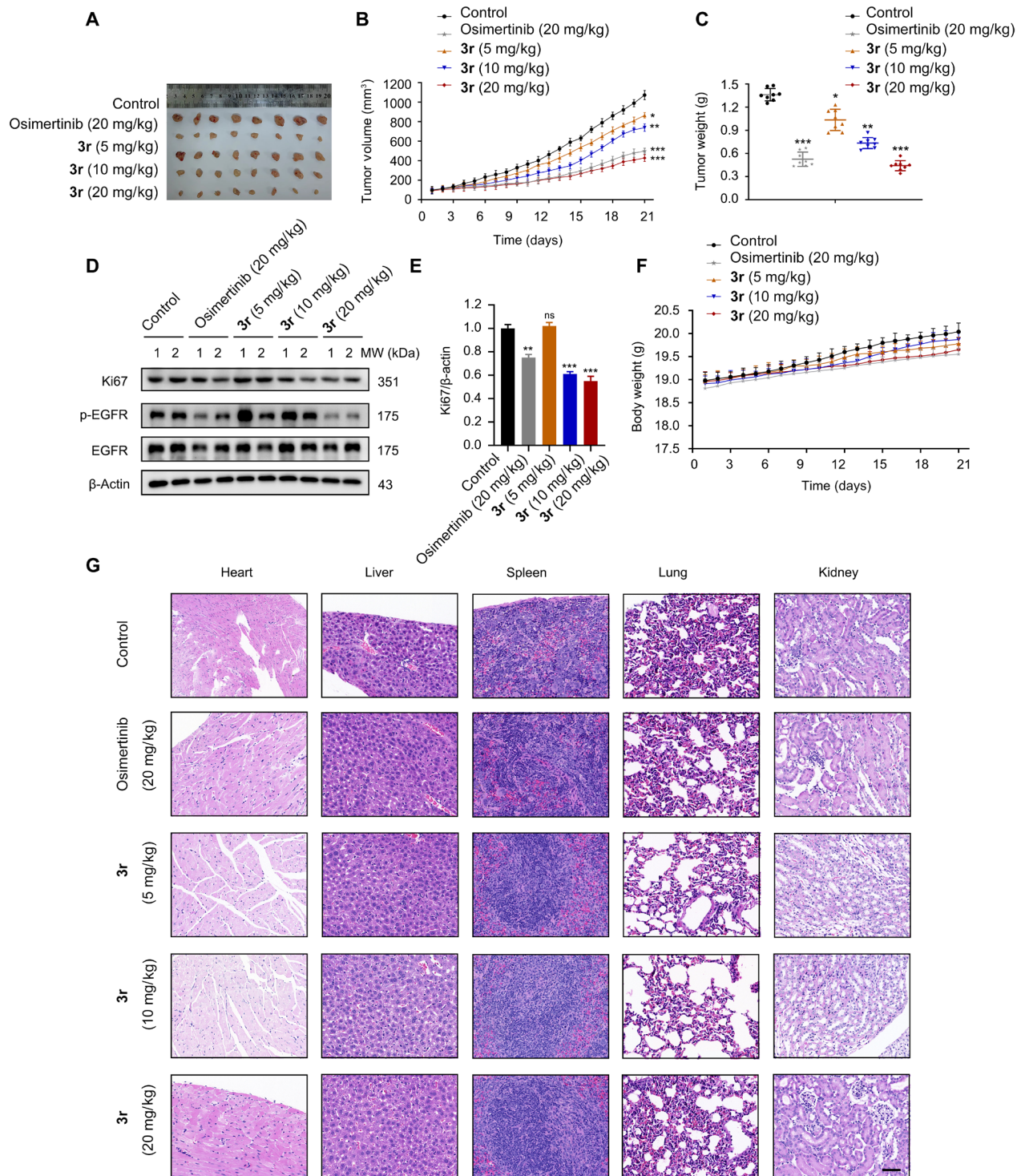


Fig. 5. In vivo antitumor effects of osimertinib and 3r on H1975 ($n = 8$ per group). (A) Tumor tissues, (B) tumor volumes, and (C) tumor weight following treatment by oral administration with osimertinib and 3r. (D) Western blot analysis of xenograft tumor tissues from vehicle-, osimertinib-, and 3r-treated nude mice for expression of Ki67, p-EGFR, and EGFR. β -Actin was used as a loading control. (E) Quantification of Ki67 by Western blot analysis. (F) Body weights following treatment by oral administration with osimertinib and 3r. (G) Representative hematoxylin and eosin staining in heart, liver, spleen, lung, and kidney sections. Scale bar, 40 μ m. Data are expressed as means \pm SEM. * $P < 0.05$, ** $P < 0.01$, *** $P < 0.001$ compared with the control groups.

Meanwhile, the compound led to the down-regulation of p-EGFR in vivo (Fig. 5D). We also found that treatment of **3r** or osimertinib did not cause obvious body weight loss and tissue damage (Fig. 5, F and G). Collectively, these results suggest that **3r** exhibits promising antitumor activity in the H1975 xenograft mouse model.

DISCUSSION

Via LSF strategy, the first example of base-controlled palladium-catalyzed regioselective Heck reaction and indole C2 C—H activation of anticancer drug osimertinib with aryl bromides is presented. By using Pd(PPh₃)₄ as a catalyst, a switchable regioselective direct arylation of osimertinib was achieved using K₂CO₃ or *t*-BuONa. Specifically, the inorganic base K₂CO₃ facilitated the arylation of the acrylamide terminal C(sp²)-H bond, while the organic base *t*-BuONa preferred the performance of indole C2 C(sp²)-H arylation. The reaction exhibited good substrate compatibility, except for heterocyclic aromatic bromides. The electronegativity or steric hindrance of the bromides did not affect the reaction, although highly hindered aromatic bromides were unable to react with the indole C2 position due to steric hindrance. On the basis of the structure-activity relationship of osimertinib, 34 acrylamide terminal double bond arylated compounds and 27 indole C2 arylated compounds were designed and synthesized. Among the arylated osimertinib derivatives, compound **3r** with the 3-fluorophenyl group at indole C2 position showed excellent in vitro activity, with similar EGFR^{T790M/L858R} inhibition and antiproliferative activity in A549 cells, as well as superior antiproliferative activity in H1975 cells than those of osimertinib. Furthermore, the in vivo antitumor efficacy of **3r** in xenograft mouse model bearing H1975 cells was also comparable to osimertinib. Overall, the strategy efficiently provides a broad range of drug derivatives in the field of medicinal chemistry, with the potential for further optimization and development of targeted therapies.

MATERIALS AND METHODS

All chemicals were obtained from commercial sources and used without further purification. The osimertinib and bromides **1a** to **1am** were purchased from Aladdin Reagent Co. Ltd. (Shanghai, P. R. China). In addition to commercially available extra dry solvents, all solvents were purified by the standard operating method. Reactions were monitored by thin-layer chromatography using 254-nm ultraviolet light to visualize the course of reactions. Flash column chromatography was performed using silica gel (200 to 300 mesh, Qingdao Haiyang Chemical Co. Ltd., Qingdao, P. R. China). NMR spectra were recorded on Bruker AV 400 MHz or 600 MHz spectrometers. Chemical shifts (δ) were reported in parts per million with tetramethylsilane as the internal standard, and *J* values were given in hertz. The following abbreviations were used to explain NMR peak multiplicities: s, singlet; d, doublet; t, triplet; m, multiplet. High-resolution mass spectra data were acquired using a Waters Acquity UPLC/Q-TOF micro mass spectrometer.

Base-controlled Pd-catalyzed arylation of osimertinib acrylamide double bond

Osimertinib (0.050 g, 0.1 mmol), Pd(PPh₃)₄ (0.012 g, 10 mol %), and K₂CO₃ (0.028 g, 0.2 mmol, 2.0 eq.) were dissolved in dry toluene (1 ml). The resulting mixture was stirred at room temperature while slowly adding the corresponding bromide. After being carried out

under an argon atmosphere at 100°C for 20 hours, the reaction was quenched with water, extracted with dichloromethane, dried over Na₂SO₄, and filtered. The filtrate was collected under reduced pressure. Further purification was performed by flash column chromatography to obtain the desired products **2a** to **2ah** (47 to 75% yields).

Base-controlled Pd-catalyzed arylation of osimertinib indole C2 position

Osimertinib (0.050 g, 0.1 mmol), Pd(PPh₃)₄ (0.023 g, 20 mol %), and *t*-BuONa (0.029 g, 0.3 mmol, 3.0 eq.) were dissolved in dry toluene (1 ml). While stirring at room temperature, the corresponding bromide (0.2 mmol, 2.0 eq.) was slowly added. The mixture was carried out under an argon atmosphere at 100°C for 20 hours. Then, the reaction was quenched with water and extracted with dichloromethane. The organic layer was dried over Na₂SO₄ and filtered, and the filtrate was collected under reduced pressure. Further purification was performed by flash column chromatography to obtain the target products **3a** to **3am** (52 to 65% yields).

Cell culture, antibodies, and reagents

A549 and H1975 cells were obtained through commercial purchase from the American Type Culture Collection (Manassas, VA, USA). All lung cancer cells were cultured in RPMI 1640 medium (Hyclone, Logan, UT, USA) supplemented with 10% fetal bovine serum. H1975OR cells were established by treating H1975 cells with increasing concentration of osimertinib, from 50 nM to 1 μ M with stepwise increments of 100 nM. MTT (M2128), Hoechst 33258 (14530), and 4',6-diamidino-2-phenylindole (DAPI) (D9542) were purchased from Sigma-Aldrich (St. Louis, MO, USA). Antibodies used in this study were as follows: Bax [5023, Cell Signaling Technology (CST)], Bcl-2 (2870, CST), caspase-3 (9662, CST), E-cadherin (14472, CST), MMP-2 (2870, CST), Ki67 (28074-1-AP, Proteintech, IL, USA), p-EGFR (3777, CST), EGFR (2085, CST), and β -actin (66009-1-Ig, Proteintech, IL, USA).

Cell viability inhibition assay

For cell viability inhibition assay, cells were seeded into 96-well plates and cultured overnight. The cells were treated with an indicated concentration of the test articles and equivalent amounts of dimethyl sulfoxide used as a negative control. After 72 hours, MTT was added, and the cells were incubated for another 4 hours. Cell viability was detected with a microplate reader at a wavelength of 490 nm.

Colony formation assay

The proliferation potential of cells was assessed by plating 1000 cells in six-well plates and treated with the indicated concentration of **3e** and **3r** or vehicle control. After 2 weeks, the cells were fixed with methanol and stained with crystal violet. The number of colonies was counted.

Hoechst 33258 staining

The H1975 cells were seeded in each well of 24-well culture plates at a density of 2×10^4 cells/ml treated or untreated with **3e**, **3r**, and osimertinib and cultured for 24 hours. The subcellular structure alterations of apoptosis were observed under a fluorescence microscope.

Annexin V/PI staining

The H1975 cells were seeded into six-well culture plates with different concentrations of **3e**, **3r**, and osimertinib and then cultured for

24 hours. The collected cells were then fixed with phosphate-buffered saline (PBS). The apoptotic ratio was measured by flow cytometry (Becton Dickinson, Franklin Lakes, NJ) after using an Annexin V/PI Staining Kit (Roche, Germany) (52).

Western blot analysis

Briefly, the H1975 cells were cultured in six-well culture plates for 24 hours. Then, cells were treated with different concentrations of **3e**, **3r**, and osimertinib. All the cells were collected and lysed by lysis buffer at 4°C for 1 hour. After 12,000 rpm centrifugation for 15 min, the protein content of the supernatant was determined by the Bio-Rad DC protein assay (Bio-Rad Laboratories, Hercules, CA, USA). Equal amounts of the total protein were separated by 10 to 15% SDS-polyacrylamide gel electrophoresis (SDS-PAGE) and transferred to polyvinylidene difluoride (PVDF) membranes, and the membranes were soaked in a blocking buffer [5% skimmed milk or bovine serum albumin (BSA)]. Proteins were detected using primary antibodies followed by horseradish peroxidase (HRP)-conjugated secondary antibodies and visualized using enhanced chemiluminescence (ECL) as the HRP substrate. All animal tumors were collected and lysed at 4°C for 1 hour. After 12,000 rpm centrifugation for 15 min, the protein content of the supernatant was determined by the Bio-Rad DC protein assay (Bio-Rad Laboratories, Hercules, CA, USA). Equal amounts of the total protein were separated by 10 to 15% SDS-PAGE and transferred to PVDF membranes, and the membranes were soaked in a blocking buffer (5% skimmed milk or BSA). Proteins were detected using primary antibodies followed by HRP-conjugated secondary antibodies and visualized using ECL as the HRP substrate (55).

Scratch assay

The H1975 cells were cultured in six-well plates and scratch-wounded by sterilized pipettes. Then, the cells were washed with PBS and cultured with normal medium or **3e**, **3r**, and osimertinib. After 24 hours of incubation, pictures were taken with a phase-contrast microscope.

Immunofluorescence analysis

Cells were seeded onto the glass coverslips in 24-well plates. After treatment with or without **3e**, **3r**, and osimertinib, cells were fixed with 4% paraformaldehyde in PBS for 30 min. The slides were then washed three times with PBS and incubated with 0.2% Triton X-100 (Sigma-Aldrich, 9002-93-1) and 5% goat serum (Sigma-Aldrich, G9023) for 30 min. Cells were incubated with indicated primary antibody overnight at 4°C and subsequently incubated with secondary antibody at room temperature for 1 hour. Nuclei were finally stained with DAPI for 5 min. Images were captured using a fluorescence microscope (56).

Xenograft mouse model

Forty female BALB/c mice (6 to 8 weeks, 20 to 22 g) were injected with H1975 cells (5×10^6 cells per mouse). When the tumor volume reached approximately 0.1 cm³, mice were randomly assigned into five groups ($n = 8$). Animals were weighed during the treatment period, and the tumor size was measured by electronic calipers during the treatment period. All mice were sacrificed, and the tumor tissues were harvested, weighed, and photographed. Then, the tumor tissues were frozen in liquid nitrogen or fixed in formalin immediately for further investigation.

Hematoxylin and eosin staining

Tissues were fixed before paraffin embedding. Then, tissues were sliced into 4 mm, stained for 5 min with hematoxylin, washed with tap water for 1 min, differentiated for 30 s (hydrochloric acid and ethanol), washed with warm water for 5 min, and finally placed into the eosin solution for 2 min before regular dehydration and sealed with resinene.

Statistical analysis

All the presented data and results were confirmed by at least three independent experiments. The data were expressed as means \pm SEM or means \pm SD and analyzed with GraphPad Prism 7.0 software. Statistical differences between two groups were determined using Student's *t* test, while between multiple groups were determined using a one-way analysis of variance. $P < 0.05$ was considered statistically significant.

Supplementary Materials

This PDF file includes:

Figs. S1 to S126
Tables S1 and S2

REFERENCES AND NOTES

- M. C. Bryan, B. Dillon, L. G. Hamann, G. J. Hughes, M. E. Kopach, E. A. Peterson, M. Pourashraf, I. Raheem, P. Richardson, D. Richter, H. F. Sneddon, Sustainable practices in medicinal chemistry: Current state and future directions. *J. Med. Chem.* **56**, 6007–6021 (2013).
- L. Costantino, D. Barlocco, Ten years of medicinal chemistry (2005–2014) in the Journal of Medicinal Chemistry: Country of contributors, topics, and public-private partnerships. *J. Med. Chem.* **59**, 7352–7359 (2016).
- I. Aliagas, R. Berger, K. Goldberg, R. T. Nishimura, J. Reilly, P. Richardson, D. Richter, E. C. Sherer, B. A. Sparling, M. C. Bryan, Sustainable practices in medicinal chemistry part 2: Green by design. *J. Med. Chem.* **60**, 5955–5968 (2017).
- G. Wu, T. Zhao, D. Kang, J. Zhang, Y. Song, V. Namasivayam, J. Kongsted, C. Pannecouque, E. D. Clercq, V. Poongavanam, X. Liu, P. Zhan, Overview of recent strategic advances in medicinal chemistry. *J. Med. Chem.* **62**, 9375–9414 (2019).
- M. Moir, J. J. Danon, T. A. Reekie, M. Kassiou, An overview of late-stage functionalization in today's drug discovery. *Expert Opin. Drug Discov.* **14**, 1137–1149 (2019).
- T. Cernak, K. D. Dykstra, S. Tyagarajan, P. Vachal, S. W. Krska, The medicinal chemist's toolbox for late stage functionalization of drug-like molecules. *Chem. Soc. Rev.* **45**, 546–576 (2016).
- L. Guillemard, N. Kaplaneris, L. Ackermann, M. J. Johansson, Late-stage C-H functionalization offers new opportunities in drug discovery. *Nat. Rev. Chem.* **5**, 522–545 (2021).
- S. D. Friis, M. J. Johansson, L. Ackermann, Cobalt-catalysed C-H methylation for late-stage drug diversification. *Nat. Chem.* **12**, 511–519 (2020).
- F. Imamura, T. Inoue, K. Kunimasa, A. Kubota, H. Kuhara, M. Tamiya, K. Nishino, M. Kimura, K. Kuno, H. Kawachi, T. Kumagai, Switching from first or second generation EGFR-TKI to Osimertinib in EGFR mutation-positive NSCLC. *Lung Cancer Manag.* **9**, LMT29 (2020).
- M. R. V. Finlay, M. Anderton, S. Ashton, P. Ballard, P. A. Bethel, M. R. Box, R. H. Bradbury, S. J. Brown, S. Butterworth, A. Campbell, C. Chorley, N. Colclough, D. A. E. Cross, G. S. Currie, M. Grist, L. Hassall, G. B. Hill, D. James, M. James, P. Kemmitt, T. Klinow-ska, G. Lamont, S. G. Lamont, N. Martin, H. L. McFarland, M. J. Mellor, J. P. Orme, D. Perkins, P. Perkins, G. Richmond, P. Smith, R. A. Ward, M. J. Waring, D. Whittaker, S. Wells, G. L. Wrigley, Discovery of a potent and selective EGFR inhibitor (AZD9291) of both sensitizing and T790M resistance mutations that spares the wild type form of the receptor. *J. Med. Chem.* **57**, 8249–8267 (2014).
- H. Akamatsu, Y. Toi, H. Hayashi, D. Fujimoto, M. Tachihara, N. Furuya, S. Otani, J. Shimizu, N. Katakami, K. Azuma, N. Miura, K. Nishino, S. Hara, S. Teraoka, S. Morita, K. Nakagawa, N. Yamamoto, Efficacy of osimertinib plus bevacizumab vs osimertinib in patients with EGFR T790M-mutated non-small cell lung cancer previously treated with epidermal growth factor receptor-tyrosine kinase inhibitor: West Japan oncology group 8715L phase 2 randomized clinical trial. *JAMA Oncol.* **7**, 386–394 (2021).
- M. Shaikh, Y. Shinde, R. Pawara, M. Noolvi, S. Surana, I. Ahmad, H. Patel, Emerging approaches to overcome acquired drug resistance obstacles to osimertinib in non-small-cell lung cancer. *J. Med. Chem.* **65**, 1008–1046 (2022).

13. B. Zhao, Z. Xiao, J. Qi, R. Luo, Z. Lan, Y. Zhang, X. Hu, Q. Tang, P. Zheng, S. Xu, W. Zhu, Design, synthesis and biological evaluation of AZD9291 derivatives as selective and potent EGFR^{L858R/T790M} inhibitors. *Eur. J. Med. Chem.* **163**, 367–380 (2019).
14. J. Shen, T. Zhang, S. J. Zhu, M. Sun, L. Tong, M. Lai, R. Zhang, W. Xu, R. Wu, J. Ding, C. H. Yun, H. Xie, X. Lu, K. Ding, Structure-based design of 5-methylpyrimidopyridone derivatives as new wild-type sparing inhibitors of the epidermal growth factor receptor triple mutant (EGFR^{L858R/T790M/C797S}). *J. Med. Chem.* **62**, 7302–7308 (2019).
15. J. Hu, Y. Han, J. Wang, Y. Liu, Y. Zhao, Y. Liu, P. Gong, Discovery of selective EGFR modulator to inhibit L858R/T790M double mutants bearing a N-9-diphenyl-9H-purin-2-amine scaffold. *Bioorg. Med. Chem.* **26**, 1810–1822 (2018).
16. B. An, T. Pan, J. Hu, Y. Pang, L. Huang, A. S. C. Chan, X. Li, J. Yan, The discovery of a potent and selective third-generation EGFR kinase inhibitor as a therapy for EGFR L858R/T790M double mutant non-small cell lung cancer. *Eur. J. Med. Chem.* **183**, 111709 (2019).
17. J. Niggenaber, L. Heyden, T. Grabe, M. P. Muller, J. Lategahn, D. Rauh, Complex crystal structures of EGFR with third-generation kinase inhibitors and simultaneously bound allosteric ligands. *ACS Med. Chem. Lett.* **11**, 2484–2490 (2020).
18. A. Ayati, S. Moghimi, S. Salarinejad, M. Safavi, B. Pouramiri, A. Foroumadi, A review on progression of epidermal growth factor receptor (EGFR) inhibitors as an efficient approach in cancer targeted therapy. *Bioorg. Chem.* **99**, 103811 (2020).
19. J. He, Z. Zhou, X. Sun, Z. Yang, P. Zheng, S. Xu, W. Zhu, The new opportunities in medicinal chemistry of fourth-generation EGFR inhibitors to overcome C797S mutation. *Eur. J. Med. Chem.* **210**, 112995 (2021).
20. B. Zhang, Z. Xu, Q. Liu, S. Xia, Z. Liu, Z. Liao, S. Gou, Design, synthesis and biological evaluation of cinnamamide-quinazoline derivatives as potential EGFR inhibitors to reverse T790M mutation. *Bioorg. Chem.* **117**, 105420 (2021).
21. K. Mishiro, R. Nishii, I. Sawazaki, T. Sofuku, T. Fuchigami, H. Sudo, N. Effendi, A. Makino, Y. Kiyono, K. Shiba, J. Taki, S. Kinuya, K. Ogawa, Development of radiohalogenated osimertinib derivatives as imaging probes for companion diagnostics of osimertinib. *J. Med. Chem.* **65**, 1835–1847 (2022).
22. M. Gunther, J. Lategahn, M. Juchum, E. Doring, M. Keul, J. Engel, H. L. Tumbrink, D. Rauh, S. Laufer, Trisubstituted pyridinylimidazoles as potent inhibitors of the clinically resistant L858R/T790M/C797S EGFR mutant: Targeting of both hydrophobic regions and the phosphate binding site. *J. Med. Chem.* **60**, 5613–5637 (2017).
23. X. E. Yan, P. Ayaz, S.-J. Zhu, P. Zhao, L. Liang, C. H. Zhang, Y.-C. Wu, J.-L. Li, H. G. Choi, X. Huang, Y. B. Shan, D. E. Shaw, C.-H. Yun, Structural basis of AZD9291 selectivity for EGFR T790M. *J. Med. Chem.* **63**, 8502–8511 (2020).
24. Q. Bai, J. Tang, H. Wang, Functionalization of sulfonamide-containing peptides through late-stage palladium-catalyzed C(sp³)-H arylation. *Org. Lett.* **21**, 5858–5861 (2019).
25. M. Shiri, M. A. Zolfigol, Surfactant-type catalysts in organic reactions. *Tetrahedron* **65**, 587–598 (2009).
26. A. H. Sandtorv, Transition metal-catalyzed C–H activation of indoles. *Adv. Synth. Catal.* **357**, 2403–2435 (2015).
27. L. Joucla, L. Djakovitch, Transition metal-catalyzed, direct and site-selective N1-, C2- or C3-arylation of the indole nucleus: 20 years of improvements. *Adv. Synth. Catal.* **351**, 673–714 (2009).
28. J. Luo, X. Xu, J. Zheng, Advance in C-H arylation of indoles. *Chin. J. Org. Chem.* **38**, 363–377 (2018).
29. M. Wu, J. Luo, F. Xiao, S. Zhang, G.-J. Deng, H.-A. Luo, Palladium-catalyzed direct and site-selective desulfitative arylation of indoles with sodium sulfinates. *Adv. Synth. Catal.* **354**, 335–340 (2012).
30. B. B. Touré, B. S. Lane, D. Sames, Catalytic C-H arylation of SEM-protected azoles with palladium complexes of NHCs and phosphines. *Org. Lett.* **8**, 1979–1982 (2006).
31. X. Wang, D. V. Gribkov, D. Sames, Phosphine-free palladium-catalyzed C-H bond arylation of free (N–H)-indoles and pyrroles. *J. Org. Chem.* **72**, 1476–1479 (2007).
32. R. J. Phipps, N. P. Grimster, M. J. Gaunt, Cu(II)-catalyzed direct and site-selective arylation of indoles under mild conditions. *J. Am. Chem. Soc.* **130**, 8172–8174 (2008).
33. L. Wang, X. Qu, Z. Li, W.-M. Peng, Rhodium-catalyzed regioselective direct C-H arylation of indoles with aryl boronic acids. *Tetrahedron Lett.* **56**, 3754–3757 (2015).
34. S.-D. Yang, C.-L. Sun, Z. Fang, B.-J. Li, Y.-Z. Li, Z.-J. Shi, Palladium-catalyzed direct arylation of (hetero)arenes with aryl boronic acids. *Angew. Chem. Int. Ed. Engl.* **47**, 1473–1476 (2008).
35. J. Zhao, Y. Zhang, K. Cheng, Palladium-catalyzed direct C-2 arylation of indoles with potassium aryltrifluoroborate salts. *J. Org. Chem.* **73**, 7428–7431 (2008).
36. X. Wang, B. S. Lane, D. Sames, Direct C-arylation of free (NH)-indoles and pyrroles catalyzed by Ar-Rh(III) complexes assembled in situ. *J. Am. Chem. Soc.* **127**, 4996–4997 (2005).
37. M. Nishino, K. Hirano, T. Satoh, M. Miura, Copper-mediated and copper-catalyzed cross-coupling of indoles and 1,3-azoles: Double C-H activation. *Angew. Chem. Int. Ed.* **51**, 6993–6997 (2012).
38. V. K. Tiwari, N. Kamal, M. Kapur, Ruthenium-catalyzed heteroatom-directed regioselective C-H arylation of indoles using a removable tether. *Org. Lett.* **17**, 1766–1769 (2015).
39. R. A. Jagtap, V. Soni, B. Punji, Expedient and solvent-free nickel-catalyzed C-H arylation of arenes and indoles. *ChemSusChem* **10**, 2242–2248 (2017).
40. X. Zhu, J.-H. Su, C. Du, Z.-L. Wang, C.-J. Ren, J.-L. Niu, M.-P. Song, Cobalt(II)-catalyzed oxidative C-H arylation of indoles and boronic acids. *Org. Lett.* **19**, 596–599 (2017).
41. S. Lakhdar, M. Westermaier, F. Terrier, R. Goumont, T. Boubaker, A. R. Ofial, H. Mayr, Nucleophilic reactivities of indoles. *J. Org. Chem.* **71**, 9088–9095 (2006).
42. Y.-S. Yang, S. Lee, S. H. Son, H.-S. Yoo, Y. H. Jang, J.-W. Shin, H.-J. Won, J. Sim, N.-J. Kim, Ligand-controlled regiodivergent direct arylation of indoles via oxidative boron Heck reaction. *Org. Chem. Front.* **9**, 5906–5911 (2022).
43. J. C. Wong, G. Z. Tang, X. H. Wu, C. G. Liang, Z. S. Zhang, L. Guo, Z. H. Peng, W. X. Zhang, X. F. Lin, Z. G. Wang, J. H. Mei, J. L. Chen, S. Pan, N. Zhang, Y. F. Liu, M. W. Zhou, L. C. Peng, W. L. Zhao, S. J. Li, C. Zhang, M. F. Zhang, Y. P. Rong, T. G. Jin, X. W. Zhang, S. Ren, Y. Ji, R. Zhao, J. She, Y. Ren, C. P. Xu, D. W. Chen, J. Cai, S. Shan, D. S. Pan, Z. G. Ning, X. P. Lu, T. P. Chen, Y. He, L. Chen, Pharmacokinetic optimization of class-selective histone deacetylase inhibitors and identification of associated candidate predictive biomarkers of hepatocellular carcinoma tumor response. *J. Med. Chem.* **55**, 8903–8925 (2012).
44. R. B. Bedford, S. J. Durrant, M. Montgomery, Catalyst-switchable regiocontrol in the direct arylation of remote C–H groups in pyrazolo[1,5-*a*]pyrimidines. *Angew. Chem. Int. Ed.* **54**, 8787–8790 (2015).
45. C. Labrière, H. Gong, B. B. Finlay, N. E. Reiner, R. N. Young, Further investigation of inhibitors of MRSA pyruvate kinase: Towards the conception of novel antimicrobial agents. *Eur. J. Med. Chem.* **125**, 1–13 (2017).
46. Y.-O. Teng, H.-Y. Zhao, J. Wang, H. Liu, M.-L. Gao, Y. Zhou, K.-L. Han, Z.-C. Fan, Y.-M. Zhang, H. Sun, Synthesis and anti-cancer activity evaluation of 5-(2-carboxyethyl)-isatin derivatives. *Eur. J. Med. Chem.* **112**, 145–156 (2016).
47. W. J. Hoekstra, H. S. Patel, X. Liang, J.-B. E. Blanc, D. O. Heyer, T. M. Willson, M. A. Iannone, S. H. Kadwell, L. A. Miller, K. H. Pearce, C. A. Simmons, J. Shearin, Discovery of novel quinoline-based estrogen receptor ligands using peptide interaction profiling. *J. Med. Chem.* **48**, 2243–2247 (2005).
48. S. Hazra, B. Mondal, R. N. Dea, B. Roy, Pd-catalyzed dehydrogenative C–H activation of iminyl hydrogen with the indole C3-H and C2-H bond: An elegant synthesis of indeno[1,2-*b*]indoles and indolo[1,2-*a*]indoles. *RSC Adv.* **5**, 22480–22489 (2015).
49. B. Alcaide, P. Almendros, M. T. Quirós, R. López, M. I. Menéndez, A. Sochacka-Ćwikła, Unveiling the reactivity of propargylic hydroperoxides under gold catalysis. *J. Am. Chem. Soc.* **135**, 898–905 (2013).
50. J. Tian, K. D. Moeller, Electrochemically assisted Heck reactions. *Org. Lett.* **7**, 5381–5383 (2005).
51. S. Wang, B. Yu, H.-M. Liu, Pd(II)-catalyzed intramolecular C(sp²)-H arylation of tryptamines using the nonsteric NH₂ as a directing group. *Org. Lett.* **23**, 42–48 (2021).
52. R. Y. Zhao, L. L. Fu, Z. X. Yuan, Y. Liu, K. Zhang, Y. M. Chen, L. M. Wang, D. J. Sun, L. X. Chen, B. Liu, L. Zhang, Discovery of a novel small-molecule inhibitor of Fam20C that induces apoptosis and inhibits migration in triple negative breast cancer. *Eur. J. Med. Chem.* **210**, 113088 (2021).
53. K. Ouyang, Z. Xi, Roles of bases in transition-metal catalyzed organic reactions. *Acta Chim. Sinica* **71**, 13–25 (2013).
54. B. S. Lane, M. A. Brown, D. Sames, Direct palladium-catalyzed C-2 and C-3 arylation of indoles: A mechanistic rationale for regioselectivity. *J. Am. Chem. Soc.* **127**, 8050–8057 (2005).
55. Y. Zhen, R. Zhao, M. Wang, X. Jiang, F. Gao, L. Fu, L. Zhang, X.-L. Zhou, Flubendazole elicits anti-cancer effects via targeting EVA1A-modulated autophagy and apoptosis in triple-negative breast cancer. *Theranostics* **10**, 8080–8097 (2020).
56. Y. Zhen, Z. Yuan, J. Zhang, Y. Chen, Y. Fu, Y. Liu, L. Fu, L. Zhang, X.-L. Zhou, Flubendazole induces mitochondrial dysfunction and DRP1-mediated mitophagy by targeting EVA1A in breast cancer. *Cell Death Dis.* **13**, 375 (2022).

Acknowledgments: L.-X. Wan (West China School of Pharmacy, Sichuan University) and Analysis and Testing Center of Southwest Jiaotong University are acknowledged for obtaining NMR and HRMS data. **Funding:** We acknowledge financial support from the National Natural Science Foundation of China (grant nos. 22277101, 22277102, 82202902, and 82003634) and the Fundamental Research Funds for the Central Universities of China (grant nos. 2682023ZTPY078, 2682023ZTPY050, and 2682023ZTPY072). **Author contributions:** F.G. designed the study. X.L., L.Z., and F.G. supervised the work. The chemical synthesis was performed by R.F. and L.S., and structural analysis was performed by J.-B.X. The biological experiments were performed by Y.-Q.Z., D.W., and L.S. All authors jointly wrote the manuscript and approved its final version. **Competing interests:** The authors declare that they have no competing interests. **Data and materials availability:** All data needed to evaluate the conclusions in the paper are present in the paper and/or the Supplementary Materials.

Submitted 22 September 2023

Accepted 5 February 2024

Published 8 March 2024

10.1126/sciadv.adl0026